Au/Rutile Catalysts: Gold Crystallites Transformation in Time at Room Temperature

Xim Bokhimi*,[1] Rodolfo Zanella[2] and Antonio Morales[1]

Universidad Nacional Autónoma de México, [1]Instituto de Física, A.P. 20-364, 01000, México D. F., Mexico; [2]Centro de Ciencias Aplicadas y Desarrollo Tecnológico, A.P. 70-186, 04510 México D. F., Mexico

Abstract: Quantitative analysis of Au/Rutile catalysts with X-ray powder diffraction showed that gold crystallites got transformed, in time, at room temperature. In this experiment, after aging the catalysts for two days, the morphology of the gold crystallites changed from a cubotahedron into a cube. This diminished the activity of the catalysts for catalyzing the oxidation of CO at temperatures below 200 ºC. On the other hand, after 5 days, the catalysts got inactivated at these temperatures. The catalyst activity correlated strongly with the gold crystallite morphology as well as its dimensions and its lattice deformations. The quantitative analysis of the catalysts suggested that the most active catalysts in the present work had gold crystallites with the morphology of a cuboctahedron with the magic number 309, and that the observed changes in the catalytic activity could be caused by defects at the boundary between the Au(100) and the Au(111) surfaces of the gold crystallites. These defects could be caused by the atomic reconstruction of the surfaces, produced by the relativistic effects on the 6s and the 5d electrons in gold atoms.

Keywords: Gold catalyst, Rutile, aging with time, Rietveld refinement, crystallite growing, Oxidation of CO, gold crystallite magic number, crystallite surface reconstruction.

INTRODUCTION

The metal particles of Au, Pt, Pd, Ir, Rh, etc. set on oxides are extensively used as heterogeneous catalysts; their catalytic activity, however, decreases when they suffer poisoning, sintering, and volatilization [1], being sintering the most common process of deactivation.

The rate and extent of sintering depend on the oxide support, the supported metal, the catalyst promoter, and the reaction temperature as well as the reaction atmosphere [2]. An interesting example of catalysts with this kind of deactivation is the gold catalyst used for the oxidation of CO a low temperatures [3-15].

The gold catalysts oxidize carbon monoxide even below 0 ºC [16,17], which makes themselves attractive for purifying air in closed places and offices as well as for reducing CO in industrial and automobile emissions, and for detecting CO [18-21]. The gold particles of these catalysts are more reactive when the support is a reducible metal oxide such as TiO_2, Co_3O_4 and Fe_2O_3 [19,22]. Also, the gold particles are highly reactive when their dimensions are between 2 and 5 nm [21-23].

Due to the low melting point of gold particles with these low dimensions, they sinter themselves easily at low temperatures limiting the practical applications of the corresponding catalysts [3-5]. Most of the gold catalysts are only active for a short period of time; a similar effect is observed when the support is MnO_x [6-8] TiO_2 [9-11] or ZrO_2 [12].

In some cases, when the reaction is carried out at room temperature, the catalytic activity decreases with time [13-15] because of the CO absorption getting into carbonates and blocking the active sites [12-14,24]; this deactivation is reversible and disappears when heating the catalyst. The agglomeration of the Au particles also deactivates the gold catalysts because it produces larger and less active gold particles [13,25-27]; this deactivation, however, is irreversible.

Some authors claim that the deactivation of gold catalysts at room temperature occurs for a local increase of temperature caused by the heat generated during the oxidation of CO and not because of the temperature of the environment [28,29].

Sintering is a major mode of deactivation for many supported catalysts, especially when the supported metal belongs to the 5d row, like the gold catalysts. These catalysts sinter with time under activation stream: at the beginning, the metal particles are highly dispersed on the support and eventually they get into their most stable energetic state (few and large metallic particles) [30-33].

It is claimed that sintering occurs mainly by the Ostwald ripening mechanism [26,31,34], even though, the particle diffusion/coalescence mechanism can be the dominant one [27,34-36].

In the case of being Au/TiO_2 catalysts, sintering is a real impediment for their industrial applications, because in these catalysts the metal normalized-area activity decreases strongly with gold particles between 2 and 6 nm.

Sintering deactivation is more dramatic in supported catalysts where the normalized-area activity remains nearly constant, for example, in supported Pt systems [17, 37].

*Address correspondence to this author at the Universidad Nacional Autónoma de México, [1]Instituto de Física, A.P. 20-364, 01000, México D. F., Mexico; Tel: +525584213048; Fax: +525556225008;
E-mail: bokhimi@fisica.unam.mx

1874-0987/09

To understand the mechanism of the gold-particles sintering in the Au/TiO_2 catalysts, in the present work, we studied the evolution of the gold crystallites in Au/Rutile catalysts at room temperature in aging time, including their catalytic activity for the oxidation of CO. This evolution was analyzed by using X-ray powder diffraction and refining the crystalline structures of both the gold phase and the support.

MATERIALS AND METHODOLOGY

Synthesis

Details about the preparation of the support and gold deposition are reported elsewhere [38]. After the support synthesis, the support was heated in air at 500 °C for 12 h.

Gold, in the concentration of 4 wt %, was supported by the deposition precipitation method with urea [38-40]. Catalyst activation was performed at 200 °C by flowing air [11] on the sample (0.6 g) at 1200 mL/min. After the activation, a portion of the catalyst was used to catalyze the oxidation of CO in the temperature range between 0 and 200 ºC. The rest of the catalyst was used to measure its X-ray powder diffraction pattern at room temperature during 2 h. Thereafter, the catalyst was kept in darkness in a dessicator until the next set of experiments was done. The catalytic properties and the diffraction patterns were measured daily for 18 days. After 233 days in the dessicator, the diffraction pattern of the catalyst was measured again to get the new gold crystallite dimensions; this catalyst was no more catalytically active below 200 °C for the oxidation of CO.

Characterization Techniques

X-Ray Powder Diffraction

The X-ray powder diffraction patterns of the catalysts were measured in air at room temperature with a Bruker D-8 Advance diffractometer with the Bragg-Brentano θ-θ geometry, CuKα radiation, a Ni 0.5 % Cu-Kβ-filter in the secondary beam and an 1-dimensional position-sensitive silicon strip detector (Bruker, Lynxeye) [41]. The diffraction intensity as a function of 2θ was measured between 20° and 110° with a 2θ step of 0.019447° for 264 s per point. The crystalline structures in the catalysts were refined using the Rietveld method with the FullProf code [42]. The crystallite size and morphology were modeled in reciprocal space with an expansion of symmetrized harmonics [43], while the lattice deformations were assumed anisotropic, and modeled with a multidimensional distribution of lattice metrics [44]. The background was modeled with a polynomial function which included the constant, the linear, the quadratic, and the cubic terms in 2θ, as well as the terms $(1/2\theta)$ and $(1/2\theta)^2$. The crystallite size distribution of rutile was simulated using the model in the FullProf code that corresponded to an isotropic microstrain contribution to the Lorentzian part of the peak profile. The standard deviations, given in parentheses in the text and the tables, show the variation in the last digit of the number. When these standard deviations correspond to Rietveld refined parameters, the values are not estimates of the probable error in the analysis as a whole, but only of the minimum possible probable errors based on a normal distribution [45].

The information about the crystallite morphology obtained from the Rietveld refinement was used to generate images of the average crystallites. This information was related to spatial positions on the average crystallite surface, therefore, they were used to generate a mesh of triangles of the surface to calculate the corresponding surface area and to render a three-dimensional image of the average crystallite, using Medit software (Release 2.3b, Feb., 2005) [46]. The connection of these triangles, with the center of the crystallite, generated a mesh of tetrahedra that was used to reckon the crystallite volume.

Catalytic Activity Measurements

The $CO + O_2$ reaction was studied between 0 and 200 °C in a flow reactor at a pressure of 1 atm. The reactant gas mixture, 1 Vol. % CO plus 1 Vol. % O_2 with a balance of N_2, flowed on the catalyst at 100 mL/min. The exit gases were analyzed with an online gas chromatograph (Agilent Technologies 6890N) equipped with flame ionization and thermal conductivity detectors.

Electron Microscopy

Catalysts were analyzed with transmission electron microscopy (TEM) in a Jeol JEM-2010F microscope. The catalyst powder was dispersed in ethanol, before placing it in the copper grid with formvar support.

RESULTS AND DISCUSSION

For the present study about the aging of Au/rutile catalysts with time, the catalyst support (rutile) was prepared at 500 ºC to have a well defined crystallite size [20]. A similar study, in a catalyst with a different support crystallite size would probably give a little different result. The aim of the present work is to show that at room temperature the properties of the gold crystallite, responsible for the catalytic activity for the oxidation of CO at low temperatures, changed because of the catalyst aging with time. These changes were quantified by using X-ray powder diffraction together with the refinement of the crystalline structures of both, the metallic gold (the active phase of the catalyst) and the support.

After the synthesis of the fresh catalyst, the catalytic activity for CO oxidation and the X-ray powder diffraction pattern were measured simultaneously in two different apparatus –In all figures, this fresh catalyst is indentified as the catalyst with 0 days aging. For all aging times, again, the catalytic activity and the X-ray diffraction pattern of the corresponding aged catalyst were also measured simultaneously. The study was performed during 233 days, but, as the main changes occurred during the first 11 aging days, we will report, mainly, the details of the observed changes for these days.

Fig. (**1**) shows the X-ray powder diffraction patterns of the catalyst as a function of aging time; the intensity of the (111) peak of metallic gold changed a little between the patterns. When the crystalline structures of the phases (metallic gold and rutile) in the catalyst were refined, it was possible to quantify the transformation of gold crystallites with aging time. This quantification supported the observed changes of the catalytic activity for the oxidation of CO at low temperatures.

For the Rietveld refinement, the rutile crystalline structure was modeled with a tetragonal unit cell, having the

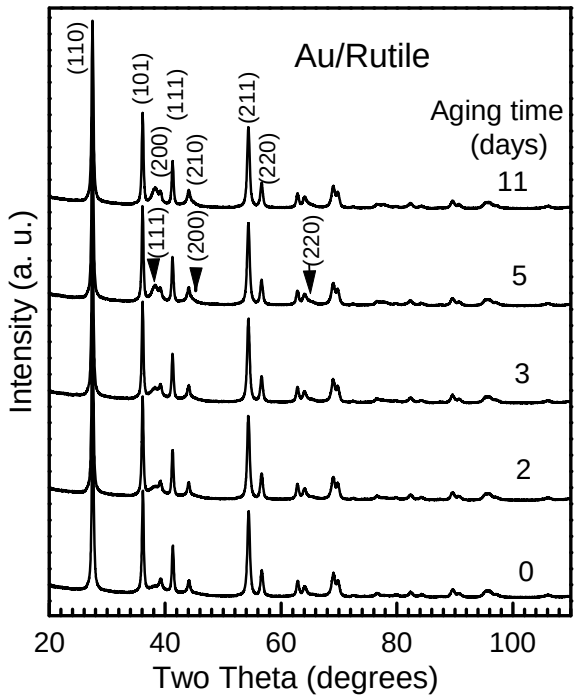

Fig. (1). X-ray diffraction patterns of the gold catalysts as a function of aging time. The Miller indices on the upper diffraction pattern correspond to rutile, and those on the second pattern (indicated by arrows) correspond to metallic gold.

symmetry of the space group $P4_2/mnm$ and a basis containing one titanium atom at the relative coordinates (0.0, 0.0, 0.0) and one oxygen atom at the relative coordinates (*x*, *x*, 0.0), with an initial *x* value of 0.3. Also, the metallic gold was modeled with a cubic unit cell, having the symmetry of the space group *Fm3m* and a basis containing only one gold atom at the relative coordinates (0.0, 0.0, 0.0).

The model used for the refinement contained the anisotropy of the crystallite dimensions and the anisotropy of the lattice deformations (microstrain). The anisotropy of crystallite dimensions was modeled in reciprocal space with an expansion of symmetrized harmonics [43], while the anisotropy of the microstrain was modeled with a multidimensional distribution of lattice metrics [44]. This gold crystallite microstrain model is only a first approximation to the real deformation in the gold crystallites, because many of these crystallites are twinned [47-48] and some others have stacking faults [49]. The small amount of gold in the catalyst, however, hindered the possibility of modeling the anisotropic microstrain using these type of crystalline defects.

Fig. (**2**) shows a typical Rietveld refinement plot; it corresponds to the fresh catalyst, which had the smallest gold crystallite (Table **1**). Although the amount of gold was small, its contribution to the diffraction pattern was big, because the atomic number of gold atoms is larger than the one of titanium and oxygen atoms (the other two chemical elements in the catalyst). This property of gold, together with the fact that the model for the contribution of rutile to the diffraction pattern is excellent, allowed us to obtain confident information about the crystallography and the microstructure of the gold crystallites, as it is shown in Fig. (**3**). It is worth to point out that in supported catalysts where the active phase and the support have similar atomic numbers the study is difficult, because the small amount of active phase.

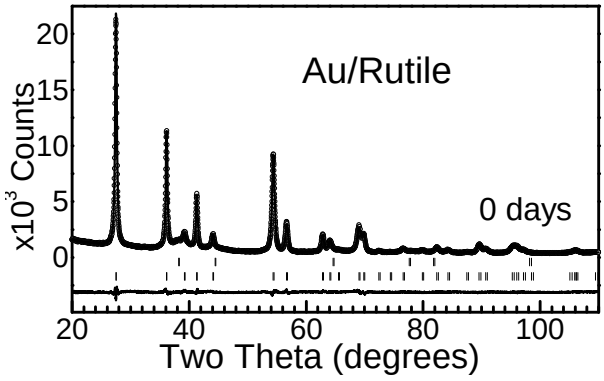

Fig. (2). Rietveld refinement plot of the gold catalyst without aging. Dots correspond to the experimental diffraction pattern; the upper continuous line corresponds to the calculated diffraction pattern, and the lower one to the difference between experimental and calculated patterns. Upper tick marks are associated to metallic gold; the lower ones to rutile.

Table 1. Gold Crystallite Dimensions in the Directions Perpendicular to (111) Plane, $G_{(111)}$, (200) Plane, $G_{(200)}$, (220) Plane, $G_{(220)}$, (311) Plane, $G_{(311)}$, and Lattice Parameter *a* as a Function of Aging Time

Aging time (days)	$G_{(111)}$ (nm)	$G_{(200)}$ (nm)	$G_{(220)}$ (nm)	$G_{(311)}$ (nm)	*a* (nm)
0	1.95	1.52	2.06	1.77	0.4078(1)
1	2.05	1.51	1.97	1.75	0.4080(1)
2	2.44	1.57	2.12	1.88	0.40781(8)
3	2.87	1.95	2.36	2.23	0.40826(7)
4	3.11	2.08	2.49	2.38	0.40823(6)
8	4.60	2.82	3.50	3.30	0.40783(1)
11	4.78	3.11	3.72	3.56	0.40793(4)
233	5.80	3.58	4.37	4.16	0.40789(3)

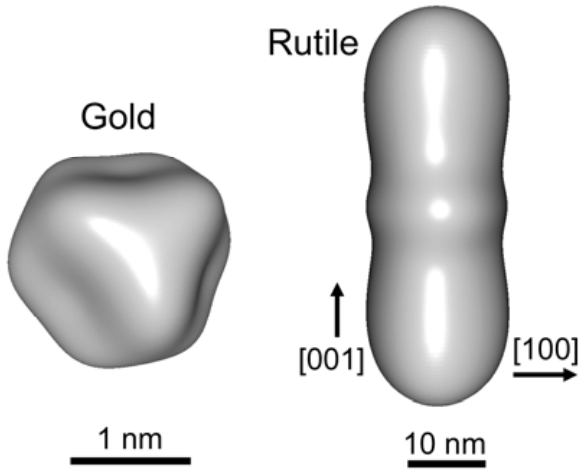

Fig. (3). Images of the average crystallites of gold and rutile got for the gold catalyst without aging.

The images of the average crystallites were constructed with the refined coefficients of the symmetrized harmonics expansion, which were used to model the average crystallite size in reciprocal space. This was done through the following mechanism: for each distance, in reciprocal space, it was associated its inverse value in real space where these inverse values were used to produce the corresponding crystallite images (Fig. **3**). The calculated images were similar to those observed in the micrographs of the catalysts obtained with transmission electron microscopy (Fig. **4**).

The crystallite images got through the analysis of the X-ray powder diffraction patterns were used to calculate other properties of the phase (Table **2**). For example, the crystallite surface area, which was calculated by triangulation of the points that defined the crystallite surface (Fig. **5A**).

This triangulation was additionally used for tetrahedralization of the crystallite volume using the following mechanism: the vertices of each triangle on the crystallite surface were joined to the center of the crystallite to generate a tetrahedron (Fig. **5B**). The sum of the volumes of all generated tetrahedra gives the total crystallite volume. This volume, together with the mass density obtained from the analysis of the X-ray diffraction patterns, was used to calculate the crystallite mass.

With all this information about the average crystallite, it was possible to calculate its specific area and the number of atoms in it (Table **2**).

The Fig. (**6**) can help readers to understand the diffraction pattern modeling during the refinement as it shows the details about the contribution of the metallic gold to the pattern (Fig. **6A**), the contribution of the background (Fig. **6B**),

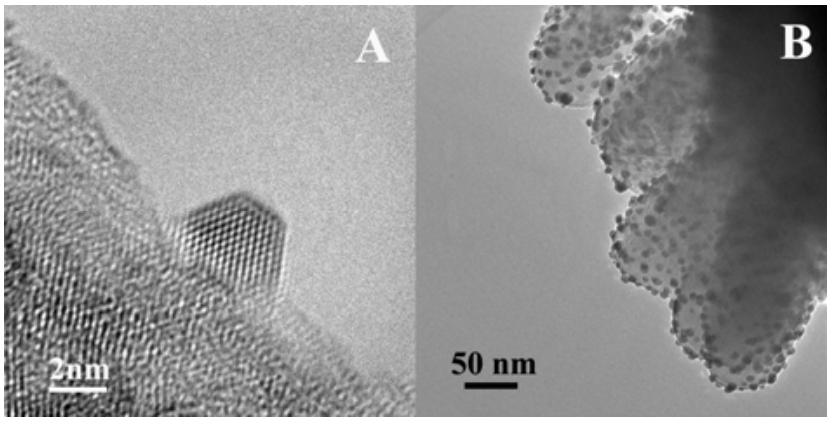

Fig. (4). TEM micrographs of the gold catalyst without aging: **A**) The small crystallite corresponds to metallic gold; **B**) the large crystallites correspond to rutile and the small on them to metallic gold.

Table 2. Gold Crystallite: Area, Volume, Number of Atoms, and Specific Area, as a Function of Aging Time

Aging time (days)	Area (nm^2)	Volume (nm^3)	Number of atoms	Specific area (m^2/g)
0	11.6	3.4	201	177
1	11.4	3.3	196	178
2	14.5	4.4	262	169
3	19.2	7.0	411	143
4	22.1	8.5	499	136
8	46.0	24.1	1420	99
11	50.8	29.0	1710	91
233	72.6	47.8	2815	79

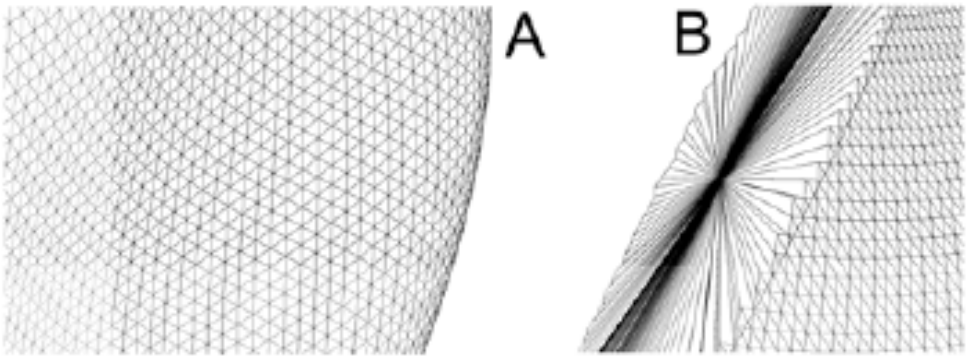

Fig. (5). **A**) Triangulation of the surface of an average crystallite; **B**) a cut of the crystallite to show the tetrahedralization of its volume.

and the curve resulting of their additions (Fig. **6C**). This illustrates the contribution of the two above mentioned parts to the total diffraction pattern, and clearly shows the origin of the shoulders of the diffraction pattern at the 2θ angles of 38.0 and 44.5 degrees, which were associated to the (111) and the (200) reflections of metallic gold.

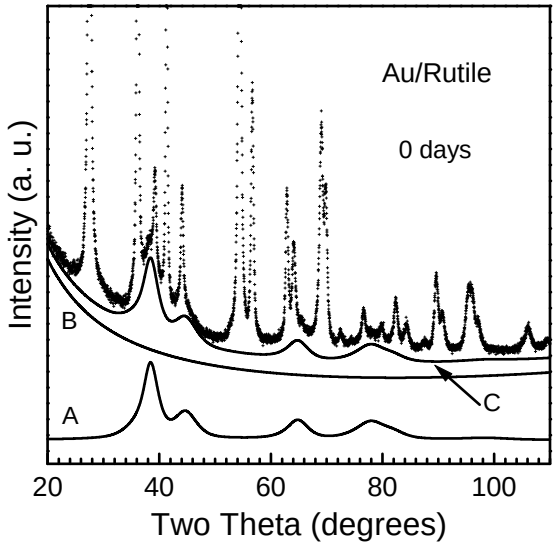

Fig. (6). Detail of the calculated contributions of gold and background to the diffraction pattern of the gold catalyst without aging.

Using the analysis of the diffraction patterns described in the previous paragraphs, we found that gold crystallites grew up in size and changed their morphology with aging time (Fig. **7** and Tables **1** and **2**). The morphology of the average gold crystallite without aging was a truncated cube that look like a cuboctahedron (Fig. **7A**); in its previous state, the crystallite might be a cuboctahedron.

When the catalyst was aged for one day the distance between the crystallite surfaces parallel to the (111) planes grew up (Fig. **7B**) –The surface parallel to (111) planes will be named, in this manuscript, the Au(111) surface. The distance between these surfaces continued growing up with time and after two days aging the average crystallite was almost a cube (Fig. **7C**). The dimension of the cube side corresponded to the distance between the crystallite surfaces that were parallel to the (200) planes (these surfaces will be named the Au(100) surfaces). This dimension was approximately the same for all the three average crystallites obtained for the aging times of 0, 1 and 2 days (Table **1**). The corresponding distance of the average crystallite after 3 days was approximately one lattice parameter (0.408 nm) larger (Table **1**).

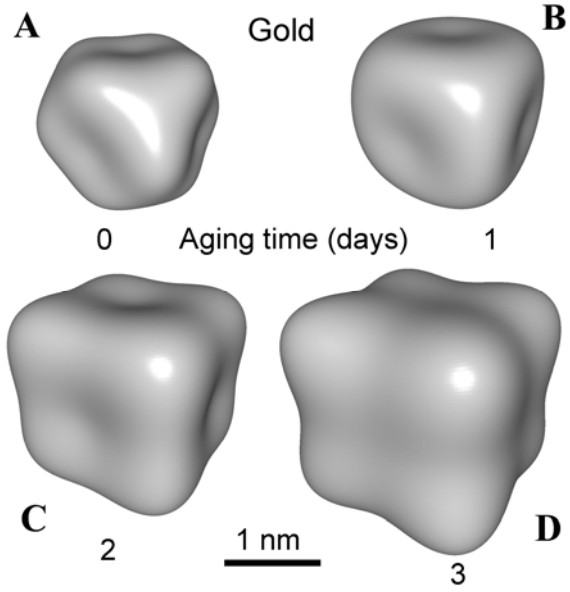

Fig. (7). Images of the gold average crystallites as a function of aging time. They were generated using the data obtained from the Rietveld refinement.

The above growing mechanism of the gold crystallites was similar to the one described in the literature for small crystallites of silver [50], in which it is published that silver crystallites grow up from a rough surface to a complete smooth surface till the crystallite gets sharp vertices. After that, the addition of more atoms, to the silver crystallite, produces an island on the last completed layer of the crystallite. This island draws atoms from the sharp corners to build a new layer that grows up until the rough corners start growing again to complete a new layer, generating a thicker crystallite with sharp corners. This last step, the last layer growing up in the silver crystallites, was also observed in the gold crystallites, studied in the present work, during the second and third aging days.

Table 3. Maximal Microstrain of Gold Crystallite Along the Direction [111], $S_{[111]}$; [200], $S_{[200]}$; [220], $S_{[220]}$; and [311] , $S_{[311]}$, as a Function of Aging Time

Aging time (days)	$S_{[111]}$ (%)	$S_{[200]}$ (%)	$S_{[220]}$ (%)	$S_{[311]}$ (%)
0	1.40	2.42	1.71	2.00
1	0.61	1.06	0.75	0.88
2	0.20	0.34	0.24	0.28

With subsequent aging, the preferential growing up of the Au(111) surfaces produced cubes with elongated vertices (Fig. **7D**), with an exaggerated elongation along the [111] direction. This could reflect, however, the degree of approximation of the model used in the Rietveld refinement for the crystallite morphology, keeping in mind that this model is not taking into account the distribution of the gold crystallite dimensions –Recently, a new model appeared considering the crystallite size distribution [51], but it is not available in the software code [42] that we used for the present work.

It is worth to highlight that the lattice deformations of the gold crystallite were larger for the smallest crystallites. These deformations decreased as the crystallite size increased (Fig. **8** and Table **3**), indicating the tendency of the atom distribution of the gold crystallites toward its most stable configuration, which corresponds to the one in the large crystallites bulk.

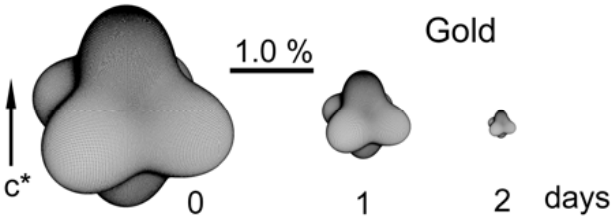

Fig. (8). Images in reciprocal space of the maximal microstrain in gold average crystallites as a function of aging time.

As the gold crystallite dimensions decreased, the proportion of atoms on the crystallite surface increased; the observed lattice deformations could reflect the large percentage of atoms on the crystallite surface.

In the literature it is reported that in large gold crystallites, the symmetry of the atom distribution on the crystallite surface deviates from the symmetry of the distribution in the bulk, producing a reconstruction of the atom distribution on the surface [52-54]. This reconstruction is due to the contraction of the 6s and the expansion of the 5d orbitals of the gold atoms, caused by the relativistic effects in this atom [55-58]. As far as this effect occurs in the interior of the gold atoms, it remains even when the atoms belong to a small gold crystallite. Therefore, it is expected that the reconstruction of the atoms on the small gold crystallite surface will produce many lattice deformations at the boundary between the Au(100) and the Au(111) surfaces of the crystallite.

The aged gold catalysts were used to catalyze the oxidation of CO in oxygen at temperatures below 200 ºC. The corresponding catalytic activity depended on aging time (Fig. **9**): after two days, the catalytic activity decreased considerably and after 5 days, the catalyst was almost inactive at 100 ºC.

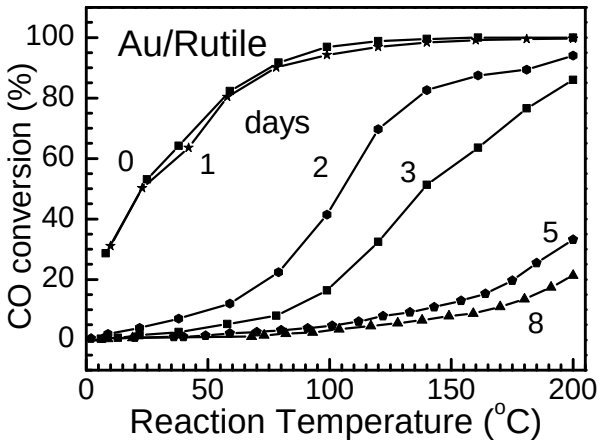

Fig. (9). CO conversion as a function of catalyst aging time.

From the description of the gold crystallites evolution with aging time in the gold catalysts described in the above paragraphs, it is drawn that the catalytic activity depends on the gold crystallite size and its morphology. The most active catalysts had gold crystallites with the morphology of a truncated cube which looked like a cuboctahedron (Figs. **7A** and **7B**).

The variation of the catalytic activity with aging time was also correlated with the amount of lattice deformations in the gold crystallite (Table **3** and Fig. **9**). For example, when the catalyst has more lattice deformations, they were more catalytically active.

The correlation between the catalytic activity and the gold crystallite morphology is stronger than the correlation between the catalytic activity and the microstrain. The catalytic activity was similar for the fresh catalyst and the catalyst aged for 1 day, as well as, their crystallite morphology and dimensions. The microstrain of the gold crystallites aged for 1 day, however, was about one half of that in the fresh catalyst, while their catalytic activity was very similar. From the above clauses, it is good to consider that the crystallite morphology and the dimensions (not the microstrain) were the responsible of the observed changes in the catalytic activity with aging time.

From the Figs. (**7** and **9**), it can be observed that the crystallites with the morphology of a truncated cube were the most active, catalytically. This morphology (rich in vertices and edges) and the reconstruction of the crystallite surfaces

generated a lot of defects at interface between the crystallite surfaces, because the atoms on the surfaces did not occupy the ideal atom positions defined by the unit cell symmetry. These defects could be the responsible of the observed catalytic activity of the gold catalyst for the oxidation of CO.

Although, the absolute dimensions of the crystallites in the present work were obtained from a rigorous analysis of the X-ray diffraction patterns, the crystallite size and microstrain distributions of the gold crystallites were not taken into account. Then the values reported in Table **1** for the crystallite dimensions can be used to analyze tendencies with aging time, as far as they are not absolute. These values, however, could change when the model used for the refinement includes new properties of the real samples, for example, the crystallite size distribution.

Because of the approximations, the reported values related to the crystallite dimensions could be omitted at the present time. They, however, give a good idea of the order of the crystallite dimensions magnitude, including the number of atoms in it. The absolute values of these parameters will certainly change in the next years when improved models for the average crystallite appear; the basic ideas of the analysis reported in the present work will also continue being valid.

The comments in the above paragraphs will help readers to understand the approximations we will do in the following analysis.

The gold crystallite dimensions perpendicular to the Au(100) surfaces were 1.520, 1.509, and 1.568 nm for the catalyst aged, during 0, 1, and 2 days, respectively; these dimensions trended to be very similar. The Table **1** shows that the lattice parameter (0.408 nm) of gold phase was nearly constant, reason why, this parameter was used to construct cubes with a side that was a multiple of it. When the multiplying factor 3, the cube side was 1.224 nm, which was smaller than the values given at the beginning of the present paragraph. The corrections of the model for the gold crystallites (for example, the crystallite size distribution) would produce larger values for the crystallite dimensions than those reported in the present work (this is because in the present work the model for the crystallite size fits to a peak broadening that was caused not only by the crystallite dimension, but also, by other factors including the size distribution). Then, it is better to construct a cube with a side of 1.632 nm, that are 4 times the lattice parameter; this side magnitude is nearer to the observed dimensions of the gold crystallites aged for 0, 1 and 2 days (Table **1**).

The above analysis shows that the three crystallites are different stages of the crystallite covering of the last crystallite surface layer, which ends forming a cube with a side of 1.632 nm.

The gold crystallite obtained after aging the catalyst for 2 days can be seen as a cube; the vertices are not sharp because the modeling of the crystallite with a finite series of symmetrized spherical functions can not generate sharp profiles. This cubic crystallite with a side of 1.632 nm contains 365 gold atoms, this number is larger than 262, which was the number of atoms obtained from the analysis of the experiments for the crystallite aged for 2 days.

It is important to notice that the truncation of the cube with a side of 1.632 nm generates the cuboctahedron with the magic number 309. This number is larger than the number of gold atoms obtained from the analysis of the catalysts aged during 0 and 1 day, which were 201 and 196, respectively (Table **2**). As it was commented in the above paragraphs, this difference can be due to an underestimation of the crystallite dimensions obtained from the Rietveld refinement.

Because the gold crystallite with side four times the lattice parameter was the final growing stage in the catalysts aged during 0 and 1 days, then its precursor crystallites were truncated cubes derived from a cube with a side that was three times the lattice parameter. This cube had a side of 1.224 nm, and contained 172 gold atoms. By truncation of this crystallite it is not possible to obtain the cuboctahedron with the magic number 147, which exists from the mathematical point of view, but cannot be generated from the crystallite growing mechanism described in above paragraphs [50]. The truncation of this cube, however, generates a truncated cube with 116 atoms, which does not correspond to the stable geometry of a cubocotahedron with a magic number. This means that during the growing process of the most external layer to generate the cube with a side of three times the lattice parameter does not exist any stable morphology.

The next step is to analyze the growing process to generate the cubic crystallite having a side of two times the lattice parameter. This cube has a side of 0.808 nm and contains 63 atoms. The truncation of this cube, which occurs by eliminating one gold atom at each corner, gives rise to the cuboctahedron with the magic number 55, which is a stable structure.

From the above analysis, it is suggested that for the present work the most active gold crystallites had an atom distribution that was near the one of the cuboctahedron with the magic number 309.

The catalyst support used in the present work was rutile prepared at 500 ºC, if it is prepared at lower temperatures the corresponding catalysts are more active for the oxidation of CO [20]; this is because the generated gold crystallites are smaller and have the morphology that looks like a cubooctahedron [20]. Then, the analysis in the above paragraphs suggests that these gold crystallites could correspond to cuboctahedra with the magic number 55.

The description of the atom distribution done along the text considered that atoms were at fixed positions, they, however, move considerably, in especial when an external molecule is near to the crystallite surface [59]. Therefore, the next step to try finding a better explanation for the catalytic activity of the gold particles during the oxidation of CO, is to consider the gold atom mobility as well as the ideal static atom positions in the crystallite.

As a final comment, it is worth to mention that after 233 days aging the crystallite dimensions were still small (Table **1**): they were only about 20 % larger than the dimensions of the crystallite obtained after 11 days aging, but large enough to lose the catalytic activity to catalyze the oxidation of CO in the presence of oxygen at room temperature. In this case, the average crystallite had the morphology of a cube with a

side 8 times the unit cell (Table **1**); this means that the side dimensions of this cube were only two times larger than those of the truncated cube associated to the average gold crystallite of the fresh catalyst.

CONCLUSIONS

The catalytic activity of the Au/Rutile catalysts depended on their aging time. The catalytic activity correlated with the changes of the gold crystallite dimensions and its morphology during the aging time. The main changes occurred along the first 5 days of the aging time. The gold crystallites grew up with the aging time in a growing mechanism, similar to the one reported in the literature related to the small crystallites of metallic silver. This mechanism describes the way of covering the crystallite last surface layer. The most catalytic active gold crystallites had the morphology of a truncated cube that looked like a cuboctahedron. The truncated-cube crystallites had a large number of vertices and edges, these and the reconstruction (caused by the relativistic effects in gold) of the crystallite surfaces produced a lot of defects that could explain the observed large catalytic activity. A critical analysis of the crystallite dimensions suggested that the most active gold crystallites in the present work could correspond to a cuboctahedron with the magic number 309. Keeping in mind that it is possible to obtain smaller gold crystallites in the gold catalysts, it is proposed that the dimensions of these crystallites could correspond to a cuboctahedron with the magic number 55. The observed evolution of the gold crystallites with time at room temperature suggests that many of the reported results in the literature about the correlation between catalytic activity and other properties can be wrong, if the corresponding measurements are not taken simultaneously in the same sample.

AKNOWLEDGEMENT

We thank M. Aguilar for technical assistance. This work was financially supported by the "Proyecto Universitario de Nanotecnología" (PUNTA) of the Universidad Nacional Autónoma de México. R. Z. is indebted to DGAPA (IN106507) and CONACYT (55154) for financial support.

REFERENCES

[1] Bartholomew, C. H. *Appl. Catal. A*, **1993**, *107*, 1.
[2] Bore, M. T.; Pham, H. N.; Switzer, E. E.; Ward, T. L.; Fukuoka, A.; Datye, A. K. *J. Phys. Chem. B*, **2005**, *109*, 2873.
[3] Pattrick, G.; van-der-Lingen, E.; Corti, C. W.; Holliday, R. J.; Thompson, D. T. *Top. Catal.*, **2004**, *30/31*, 273.
[4] Haruta, M.; Daté, M. *Appl. Catal. A*, **2001**, *222*, 427.
[5] Yan, W. F.; Mahurin, S. M.; Overbury, S. H.; Dai, S. *Top. Catal.*, **2006**, *39*, 199.
[6] Hoflund, G. B.; Gardner, S. D.; Schryer, S. D. *Appl. Catal. B*, **1995**, *6*, 117.
[7] Hoflund, G. B.; Gardner, S. D. *Langmuir*, **1995**, *11*, 3431.
[8] Wang, G. Y.; Zhang, W. X.; Jiang, D. Z. *Acta Chim. Sin.*, **2000**, *5*, 752.
[9] Grunwaldt, J.-D.; Baiker, A. *J. Catal.*, **1999**, *181*, 223.
[10] Zanella, R.; Louis, C. *Catal. Today*, **2005**, *107-108*, 768.
[11] Bollinger, M. A.; Vannice, M. A. *Appl. Catal. B*, **1996**, *8*, 417.
[12] Knell, A.; Barnickel, P.; Baiker, A.; Wokaun, A. *J. Catal.*, **1992**, *137*, 306.
[13] Konova, P.; Naydenov, A.; Venkov, C.; Mehandjiev, D.; Andreeva, D.; Tabakova, T. *J. Mol. Catal. A*, **2004**, *213*, 235.
[14] Schubert, M. M.; Venugopal, A.; Kahlich, M. J.; Plzak, V.; Behm, R. J. *J. Catal.*, **2004**, *222*, 32.
[15] Schubert, M. M.; Plzak, V.; Garche, J.; Behm, R. J. *Catal. Lett.*, **2001**, *76*, 143.
[16] Haruta, M.; Kobayashi, T.; Sano, H.; Yamada, N. *Chem. Lett.*, **1987**, *2*, 405.
[17] Haruta, M. *Chem. Rec.*, **2003**, *3*, 75.
[18] Anderson, J. A. *J. Chem. Soc. Faraday Trans.*, **1992**, *88*, 1201.
[19] Haruta, M.; Tsubota, S.; Kobayashi, T.; Kageyama, H.; Genet, M. J.; Delmon, B. *J. Catal.*, **1993**, *144*, 175.
[20] Bokhimi, X.; Zanella, R.; Morales, A. *J. Phys Chem. C*, **2007**, *111*, 15210.
[21] Zanella, R.; Giorgio, S.; Shin, C. H.; Henry, C. R.; Louis, C. *J. Catal.*, **2004**, *222*, 357.
[22] Bond, G. C.; Thompson, D. T. *Catal. Rev.-Sci. Eng.*, **1999**, *41*, 319.
[23] Janssens, T. V. W.; Clausen, B. S.; Hvolbaek, B.; Falsig, H.; Christensen, C. H.; Bligaard, T.; Norskov, J. K. *Top. Catal.*, **2007**, *44*, 15.
[24] Wang, G. Y.; Lian, H. L.; Zhang, W. X.; Jiang, D. Z.; Wu, T. H. *Kinet. Catal.*, **2002**, *43*, 433.
[25] Andreeva, D. *Gold Bull.*, **2002**, *35*, 82.
[26] Kolmakov, A.; Goodman, D. W. *Catal. Lett.*, **2000**, *70*, 93.
[27] Kielbassa, S.; Kinne, M.; Behm, R. J. *J. Phys. Chem. B*, **2004**, *108*, 19184.
[28] Bond, G. C.; Louis, C.; Thompson, D. T. *Catalysis by Gold*, 1st ed.; Imperial College Press: London, **2006**; Vol. *6*.
[29] Moreau, F.; Bond, G. C. *Top. Catal.*, **2007**, *44*, 95.
[30] McVicker, G. B.; Garten, R. L.; Baker, R. T. *J. Catal.*, **1978**, *54*, 129.
[31] Lai, X.; Goodman, D. W. *J. Mol. Catal. A*, **2000**, *162*, 33.
[32] Wynblatt, P.; Gjostein, N. A. *Progress in Solid State Chemistry*, Elsevier Science: Amsterdam, **1975**; Vol. *9*.
[33] Cosandey, F.; Madey, T. E. *Surf. Rev. Lett.*, **2001**, *8*, 73.
[34] Mitchell, C. E. J.; Howard, A.; Carney, M.; Egdell, R. G. *Surf. Sci.*, **2001**, *490*, 196.
[35] Sykes, E. C. H.; Williams, F. J.; Tikhov, M. S.; Lambert, R. M. *J. Phys. Chem. B*, **2002**, *106*, 5390.
[36] Kolmakov, A.; Goodman, D. W. *Chem. Rec.*, **2002**, *2*, 446.
[37] Parker, S. C.; Campbell, C. T. *Phys. Rev. B* **2007**, *75*, 035430.
[38] Bokhimi, X.; Zanella, R.; Morales, A. *J. Phys Chem. C*, **2008**, *112*, 12463.
[39] Zanella, R.; Giorgio, S.; Henry, C. R.; Louis, C. *J. Phys. Chem. B*, **2002**, *106*, 7634.
[40] Zanella, R.; Delannoy, L.; Louis, C. *Appl. Catal. A*, **2005**, *291*, 62.
[41] Dabrowski, W.; Grybos, P.; Hottowy, P.; Swientek, K.; Wiacek, P. *Nuclear Inst. Methods Phys. Res. A*, **2003**, *512*, 213.
[42] Rodriguez-Carbajal, J. Laboratoire Leon Brilloin (CEACNRS): Saclay, France, **2006**.
[43] Jarvinen, M. *J. Appl. Crystallogr.*, **1993**, *26*, 525.
[44] Stephens, P. W. *J. Appl. Crystallogr.*, **1999**, *32*, 281
[45] Prince, E. *J. Appl. Crystallogr.*, **1981**, *14*, 157.
[46] Medit software: "le logiciel a été conçu et réalisé au laboratoire Jacques Luois Lions de l'Université Pierre et Marie CURIE (Paris 6)". Laboratoire Jacques Louis Lions, Boite Courrier 187, 75252 Paris cedex 05, France. **2004**.
[47] Marks, L. D. *Surf. Sci.*, **1985**, *150*, 302.
[48] Slouf, M.; Kuzel, R.; Matej, Z. *Z. Krystallogr. Suppl.*, **2006**, *23*, 319.
[49] Hofmeister, H.; Haefke, H.; Krohn, M. *J. Cryst. Growth*, **1982**, *58*, 507.
[50] Tersoff, J.; Denier van de Gon, A.W.; Tromp, R. M. *Phys. Rev. Lett.*, **1993**, *70*, 1143.
[51] Popa, N. C.; Balzar, D. *J. Appl. Crystallogr.*, **2008**, *41*, 615.
[52] Harten, U.; Lahee, A. M.; Toennies, J. P.; Woll, C. *Phys. Rev. Lett.*, **1985**, *54*, 2619.
[53] Marks, L. D.; Heine, V.; Smith, D. J. *Phys. Rev. Lett.*, **1984**, 656.
[54] Mochrie, S. G. J.; Zehner, D. M.; Ocko, B. M.; Gibbs, D. *Phys. Rev. Lett.*, **1990**, *64*, 2925.

[55] Takeuchi, N.; Chan, C. T.; Ho, K. M. *Phys. Rev. B,* **1991**, *43*, 14363.
[56] Pyykko, P.; Desclaux, J.-P. *Acc. Chem. Res.*, **1979**, *12*, 276.
[57] Pyykko, P. *Angew. Chem. Int. Ed.*, **2002**, *41*, 3573.
[58] Gorin, D. J.; Toste, F. D. *Nature*, **2007**, *446*, 395.
[59] Somorjai, G. A.; Van Hove, M. A. *Acta Crystallogr. B,* **1995**, *51*, 502.

Received: February 11, 2009 Revised: March 13, 2009 Accepted: March 13, 2009